Smart Structures and Systems, *Vol. 32, No. 4 (2023) 253-266*
https://doi.org/10.12989/sss.2023.32.4.253

Pipeline defect detection with depth identification using PZT array and time-reversal method

Yang Xu*[1], Mingzhang Luo [1a] and Guofeng Du [2b]

[1] *Department of Automation, School of Electronic Information and Electrical Engineering, Yangtze University, Jingzhou, Hubei, 434023, China*
[2] *Department of Civil and Engineering Management, School of Urban Construction, Yangtze University, Jingzhou, Hubei, 434023, China*

(*Received June 13, 2022, Revised October 8, 2023, Accepted October 12, 2023*)

Abstract. The time-reversal method is employed to improve the ability of pipeline defect detection, and a new approach of identifying the pipeline defect depth is proposed in this research. When the L(0,2) mode ultrasonic guided wave excited through a lead zirconate titinate (PZT) transduce array propagates along the pipeline with a defect, it will interact with the defect and be partially converted to flexural F(n, m) modes and longitudinal L(0,1) mode. Using a receiving PZT array attached axisymmetrically around the pipeline, the L(0,2) reflection signal as well as the mode conversion signals at the defect are obtained. An appropriate rectangle window is used to intercept the L(0,2) reflection signal and the mode conversion signals from the obtained direct detection signals. The intercepted signals are time reversed and re-excited in the pipeline again, result in the guided wave energy focusing on the pipeline defect, the L(0,2) reflection and the L(0,1) mode conversion signals being enhanced to a higher level, especially for the small defect in the early crack stage. Besides the L(0,2) reflection signal, the L(0,1) mode conversion signal also contains useful pipeline defect information. It is possible to identify the pipeline defect depth by monitoring the variation trend of L(0,2) and L(0,1) reflection coefficients. The finite element method (FEM) simulation and experiment results are given in the paper, the enhancement of pipeline defect reflection signals by time-reversal method is obvious, and the way to identify pipeline defect depth is demonstrated to be effective.

Keywords: defect detection; lead zirconate titinate (PZT) array; pipeline; time-reversal method; ultrasonic guided wave

1. Introduction

Common metal defects, such as corrosion and cracks, are major safety hazards in the operation of industrial pipelines (Hong *et al*. 2016a, b, Cahill *et al*. 2018, Feng *et al*. 2017). Ultrasonic guided wave, as a nondestructive detection technology, has been widely employed in many structure health monitoring, including pipeline (Garg *et al*. 2016, Beena *et al*. 2017, Gomez *et al*. 2017, Niu *et al*. 2018, Li *et al*. 2020). It is important to identify the defect characteristics in the process of pipeline defect inspection. Scholars have carried out research to study the interaction between guided wave and defects in pipeline. Gazis (1959a) firstly and completely derived the theoretical expression of guided wave propagation in an infinitely length and isotropic hollow cylindrical shell and carried out the numerical computation, which lays theoretical foundation for the study of the guided wave in the pipeline. Fitch and Arthur (Fitch 1963) carried out experimental studies and obtained the values of group velocity, which verified the theoretical solution of Gazis. The FEM simulation combined with experimental verification are commonly used in pipeline structural health monitoring. Alleyne and Cawley (Alleyne and Cawley 1996, 1997) studied the reflection of L(0,2) mode guided wave at circumferential notches in a pipe by using FEM simulation and experiments. Cawley *et al*. (2002) studied the reflection signals of extensional guided waves from notches of different axial, circumferential and through-thickness dimensions in pipes. Lowe *et al*. (1998a) investigated the mode conversion of longitudinal guided waves at the pipe defects. Some scholars (Wang *et al*. 2009; Wang and Hao 2014; Li *et al*. 2014; Zhang *et al*. 2018) have also studied the structure damage detection using guided wave, including pipeline defect detection (Wang *et al*. 2010; Lovstad and Cawley 2011; Ratassepp *et al*. 2010).

Usually, the reflection signal from small defect is weak and difficult to distinguish. To improve the inspection ability of guided waves for small defect, time-reversal method has been introduced to the field of ultrasonic guided wave detection (Fink 1992, Wu *et al*. 1992, Cassereau and Fink 1992, Ing and Fink 1998, May and Dual 2006, Zadeh *et al*. 2016), and lots of research results have provided useful references for this new technology (Núñez and Negreira 2005, Gao *et al*. 2015, Leutenegger and Dual 2002, Liao *et al*. 2009). Deng *et al*. (2010) studied the temporal-spatial focusing effect of time-reversal method on the pipeline defect detection. Zhou (2012) investigated the realization of guided wave inspection instrument using time-reversal method. Fu *et al*. (2013) proposed a synthetic time-reversal method which provides an effective means of application in engineering. Xu *et al*. (2019) proposed a

*Corresponding author, Ph.D.,
E-mail: xuyang@yangtzeu.edu.cn
[a] Professor, E-mail: lmz@yangtzeu.edu.cn
[b] Professor, E-mail: gfdu@yangtzeu.edu.cn

ISSN: 1738-1584 (Print), 1738-1991 (Online)

method of pipeline defect localization using time-reversal and matching pursuit algorithm. Du *et al*. (2016) used time reversal method to conduct pipeline corrosion pit monitoring test.

The Lead Zirconate Titinate (PZT) with strong piezoelectric effect is the most commonly used piezoceramic material (Luo *et al*. 2016, Xu *et al*. 2018, Giannelli *et al*. 2017). PZT transducers are widely utilized in the ultrasonic guided wave based health monitoring of various structures (Wang *et al*. 2019, Huo *et al*. 2017, Lu *et al*. 2017, Hosseinabadi *et al*. 2014, Jiang *et al*. 2017, Du *et al*. 2017). In this research, two PZT transducer arrays are arranged at the end of the pipeline axisymmetrically to excite and receive ultrasonic guided wave in the process of pipeline defect detection. When the excited L(0,2) mode guided wave propagates along the pipe with a defect, it will interact with the defect and be partially converted to flexural F(n,m) modes as well as longitudinal L(0,1) mode (Tang *et al*. 2007). The L(0,2) reflection and the mode conversion signals at the defect are obtained from the receiving PZT array, and these detection signals are intercepted with an appropriate rectangle window. The intercepted signals are time reversed and re-excited in the pipeline again, leads to the wave energy focusing on the defect, and result in the L(0,2) and L(0,1) reflection signals being enhanced to a higher level. The enhancement of L(0,2) and L(0,1) reflection signals at defect is investigated by FEM simulation and experimental verification. Besides the L(0,2) reflection mode, the L(0,1) conversion mode also contains useful pipeline defect information. Define the reflection coefficient as the ratio of the Peak to Peak value of the reflected signal to that of the excitation signal. The L(0,2) and L(0,1) reflection coefficient varies with different pipeline defect depth. The variation trend of L(0,2) and L(0,1) reflection coefficients provides an important reference for pipeline defect depth identification.

2. Theory fundamentals

2.1 Basic equations of guided wave in pipeline

The propagation characteristics of guided waves in an infinite, axisymmetric, and perfectly elastic pipe is investigated by using the cylindrical coordinate system, as shown in Fig. 1. Assume that the inner and outer radii of the pipe are a and b, respectively. When the guided waves propagate in the pipe, the particle displacements satisfy the Navier equations (Gazis 1958, Jiang *et al*. 2014, Yan *et al*. 2018)

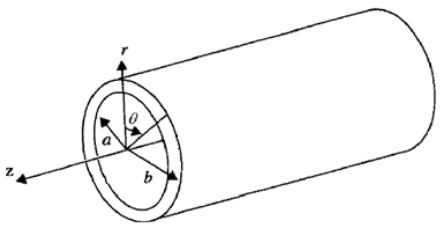

Fig. 1 The cylindrical reference coordinate system

$$\mu\nabla^2 U + (\lambda+\mu)\nabla(\nabla\cdot U) = \rho\frac{\partial^2 U}{\partial t^2} \tag{1}$$

where $\boldsymbol{U}$ is displacement vector; t is time; λ and $\mu$are the Lame constants of pipe material; ρ is the density of material; and ∇^2 is the Laplace operator.

Based on the Helmholtz decomposition law, the displacement vector $\boldsymbol{U}$ can be decomposed into an expansion scalar potential function$\varphi$and an equal volume vector potential function $\boldsymbol{H}$, as show in following

$$\begin{cases} U = \nabla\varphi + \nabla\times H \\ \nabla\cdot H = 0 \end{cases} \tag{2}$$

where the potential function φ and $\boldsymbol{H}$ satisfy the wave equation

$$\begin{cases} \nabla^2\varphi = \dfrac{1}{{c_p}^2}\dfrac{\partial^2\varphi}{\partial t^2} \\ \nabla^2 H = \dfrac{1}{{c_s}^2}\dfrac{\partial^2 H}{\partial t^2} \end{cases} \tag{3}$$

where $c_p$and $c_s$are P-wave and S-wave velocity in an elastic medium, respectively.

When air is filled inside the pipe, the stresses on the inner and outer surfaces satisfy the following boundary conditions

$$\sigma_{rr}|_{r=a,b} = \sigma_{r\theta}|_{r=a,b} = \sigma_{rz}|_{r=a,b} = 0 \tag{4}$$

The final displacement, stress and potential function can be obtained by solving the above wave equation. Substituting the boundary conditions, the following linear equations are obtained

$$[c_{ij}]_{6\times6}[A\ B\ A_1\ B_1\ A_2\ B_2]^T = [0\ 0\ 0\ 0\ 0\ 0]^T \tag{5}$$

To ensure non-zero solution to equation (5), the coefficients determinant must be zero

$$\left|c_{ij}\right|_{6\times6} = 0,\ (i,j = 1\text{ to }6) \tag{6}$$

where c_{ij} is related to the frequency, wave number, the pipe diameter, Lames constant, pipe material Poisson's ratio and density.

Eq. (6) is the dispersion equation of the guided wave in the hollow tubular, and Gazis (1959b) firstly derived the exact solution under free boundary conditions. There are different modes of propagation when ultrasonic guided wave propagates axially in a hollow cylinder: the axisymmetric longitudinal mode L(0,m), the axisymmetric torsional mode T(0,m), and the non-axisymmetric flexual mode F(n,m). By numerically solving the dispersion Eq. (6), the dispersion curve can be plotted, and different modes can be determined from the dispersion curves (Yan *et al*. 2012).

A 2000mm-long AISI304 steel pipe is used in this research, and its inner and outer diameters are 68 mm and 76 mm, respectively. The corresponding dispersion curves are shown in Fig. 2. In 70 kHz to 200 kHz frequency range, the L(0,2) mode has the fastest group velocity, and its

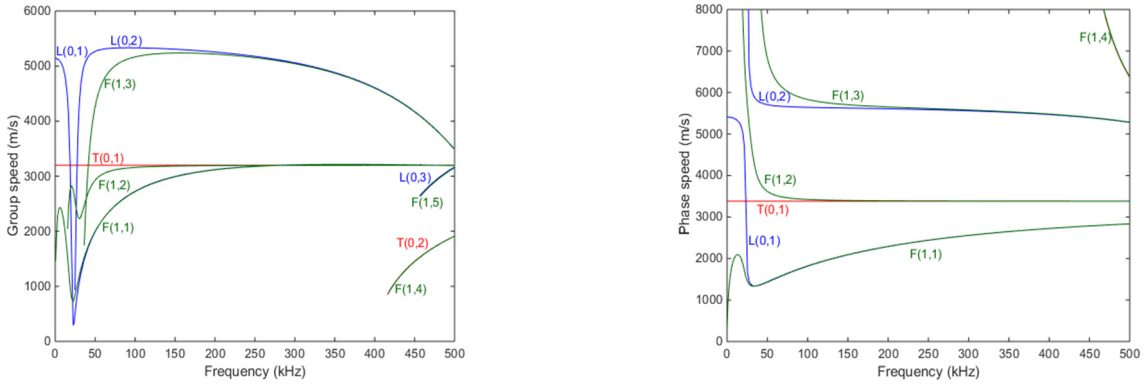

(a) Group velocity dispersion curves (b) Phase velocity dispersion curves

Fig. 2 Dispersion curves for the AISI304 steel pipe

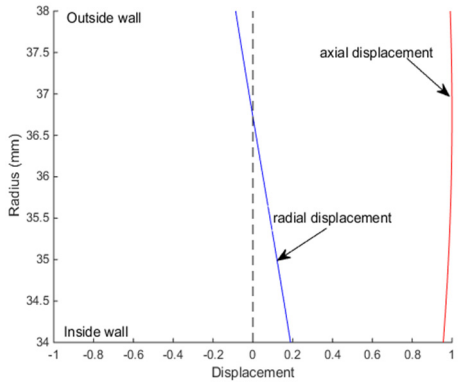

Fig. 3 Displacement profile of L(0,2)

dispersion is very slight. So that the L(0,2) mode is mostly utilized for pipeline defect detection in practice.

Analyzing the displacement profile of guided waves plays an important role in choosing appropriate guided wave modes for pipeline defect detection (Lowe *et al.* 1998b). The displacement profile for the L(0,2) mode in the steel pipe at the frequency of 120 kHz is shown in Fig. 3, which shows that the axial displacement is distributed uniformly and relatively larger along the pipe wall. This is beneficial to detect any defect on the cross section of the pipe. The radial displacement is smaller, and the energy loss is small in the propagation process. If the excitation signal vibrates axially in a pipe, the L(0,2) mode will be generated.

The displacement profile for L(0,1) mode in the steel pipe at the frequency of 120 kHz is shown in Fig. 4. It can be seen that the axial displacement of L(0,1) mode varies in the direction of wall thickness, and both forward and backward displacement exist. The radial displacement is relatively larger along the pipe wall. If the excitation signal vibrates radially in a pipe, the L(0,1) mode will be generated.

In this research, we hope to excite single pure L(0,2) mode for pipeline defect detection, and the excitation of L(0,1) mode should be restrained. There are several kinds of methods to suppress the undesired mode in the procedure of signal excitation. To strengthen the excitation of L(0,2) mode as well as to restrain that of the L(0,1) mode, the axially vibrating PZT patch should be used. According to Alleyne and Cawley (Alleyne and Cawley 1996, 1997), it is possible to suppress the excitation of L(0,1) mode by adjusting the length of the PZT patch to be an entire wavelength of L(0,1) mode at specific frequency. In this research, an 120 kHz Hanning windowed toneburst signal is applied to the surface-bonded PZT array at one end of the pipe to excite L(0,2) mode guided wave. It is know from the phase velocity dispersion curves shown in Fig. 2(b) that the L(0,1) mode phase velocity at 120 kHz is about 1937m/s, so that the L(0,1) mode wave length is calculated as

$$\lambda = \frac{1937}{120 \times 10^3} = 16\text{mm} \tag{7}$$

Therefore, choosing 16 mm long length-expanding and contracting piezoelectric elements to compose a transmitting transducer array, and arrange this array at one end of the pipe. Then the single pure L(0,2) mode guided wave can be excited by applying a Hanning windowed toneburst signal centered on the 120 kHz frequency to this transducer array.

2.2 The influence of defect depth on L(0,2) to L(0,1) mode conversion

According to Ditri (1994), the shape and size characteristics of defect directly determine the guided wave

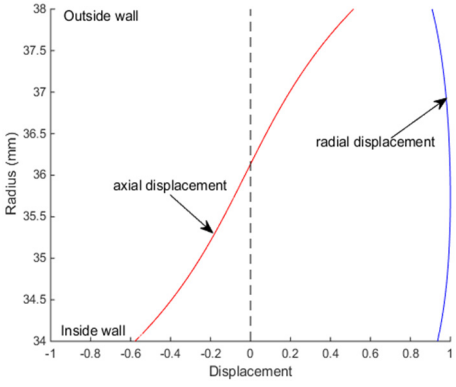

Fig. 4 Displacement profile of L(0,1)

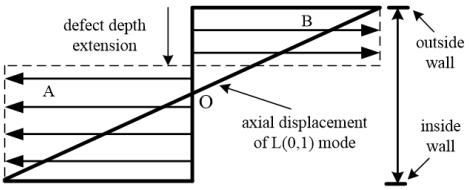

(a) The axial displacement profile of L(0,1) mode and A, B components

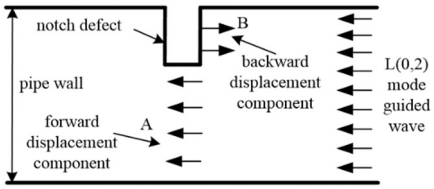

(b) Schematic pipe wall with a notch defect

Fig. 5 The influence of defect on the displacement distribution in pipe wall

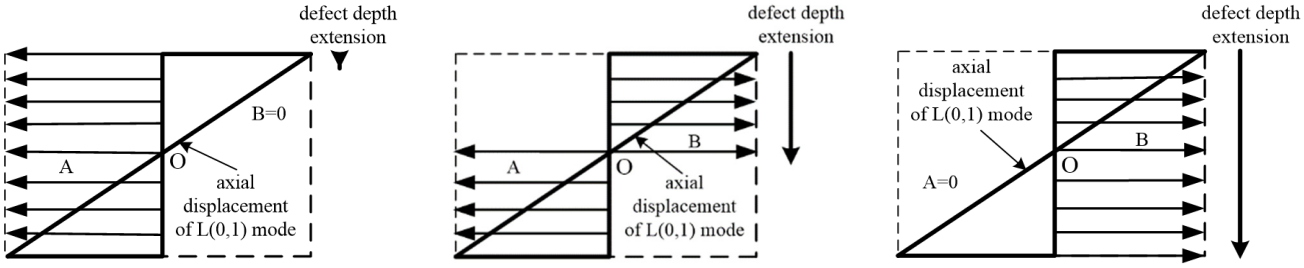

(a) Zero-depth defect, A = maximum, B = 0

(b) Half-wall-thickness defect, A = B

(c) Through-thickness defect, A = 0, B = maximum

Fig. 6 The L(0,1) mode conversion trend in pipe wall

mode conversion. When the excited incident L(0,2) mode guided wave propagates along the pipe with a notch defect, it will interact with the defect and be partially converted to non-axisymmetric flexural F(n,m) modes and axisymmetric longitudinal L(0,1) mode, and the L(0,1) conversion mode varies with the defect depth. The following illustrate the influence of defect depth on L(0,2) to L(0,1) mode conversion. The axial displacement profile of L(0,1) mode is shown in Fig. 5(a), and the axial displacement zero location is labeled O. If both the forward and the backward displacement components, labeled respectively as A and B, exist in the pipe wall, the L(0,1) mode guided wave will be generated.

As illustrated in Fig. 5(b), when the L(0,2) mode guided wave propagates along the pipe, there is only one uniform forward displacement in the pipe wall before a notch defect is encountered. When encountering a not-through-thickness notch defect, the L(0,2) mode guided wave will be scattered. Some of L(0,2) mode guided waves will continue to propagate forward after the defect, still showing forward displacement A. The other portion of L(0,2) mode guided waves will be reflected from the defect and propagate backward, showing backward displacement B. At this moment, the displacement profile in the pipe wall is similar to that of the L(0,1) mode, therefore, some of L(0,2) mode guided waves will be converted to L(0,1) mode at the defect. If there is no defect in the pipe, the percentage of displacement component B is zero. If the defect in the pipe reached through-thickness, the percentage of displacement component A is zero. In these two extreme cases, the displacement profiles are not consistent with that of the L(0,1) mode, so that the L(0,2) to the L(0,1) mode conversion will not took place. If the defect in the pipe has not yet reached through-thickness, the displacement components A and B will exist simultaneously, and the displacement profile is similar to that of L(0,1) mode. In such a situation, the reflected signals at defect will contain the L(0,1) conversion mode.

The variation trend of L(0,1) mode conversion in the pipe wall is shown in Fig. 6. As illustrated in Fig. 6(a), when the defect depth is zero (no defect in the pipe), there is only forward displacement component A in pipe wall. At this moment, there is no L(0,1) mode in the pipe. With the defect depth extends further, the percentage of the backward displacement component B increases. From this time on, the displacement profile in pipe wall gradually matches that of the L(0,1) mode, thus the L(0,1) mode emerges, and the amplitude of L(0,1) mode waveform will increase. As illustrated in Fig. 6(b), when the defect depth extends to half-wall-thickness, both forward displacement component A and backward displacement component B are the most similar to that of the L(0,1) mode. At this moment, the amplitude of the L(0,1) mode waveform reaches the maximum value. As illustrated in Fig. 6(c), when the defect depth extends to through-thickness, the percentage of the backward displacement component B continuously increases to the maximum value, while the percentage of the forward displacement component A decreases to zero. Accordingly, the amplitude of the L(0,1) mode waveform gradually decrease and eventually reaches zero. The entire process results in the amplitude of the L(0,1) mode waveform increasing first, then decreasing, and at last reaching zero. Therefore, the variation trend of L(0,1) mode waveform amplitude could be used to identify the pipe defect depth.

2.3 The synthetic time-reversal method

When using guided wave in pipeline defect inspection, the time-reversal method can be used to improve the ability

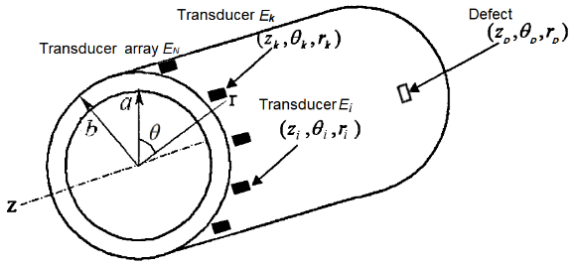

Fig. 7 Schematic of pipe with a single defect and a transducer array

of small defect detection (Deng *et al*. 2010). General time-reversal method requires a multi-channel synchronous excitation-reception system to fulfill two synchronous excitations, and this is complicated as well as inconvenient. In this research a new approach of synthetic time-reversal method is used instead. The synthetic time-reversal is a signal processing method that employs the single-channel apparatus to synthesize the multi-channel synchronous excitation system (Fu *et al*. 2013).

As shown in Fig. 7, (z_D, θ_D, r_D) denotes the pipe defect, (z_i, θ_i, r_i) and (z_k, θ_k, r_k) represent the central position of transducer E_i and E_k (i, k = 1, 2, 3,…, N) in an array of N transducers uniformly distributed along the pipe circumference, respectively. The transducer array E_N is utilized to excite and to receive guided wave for pipe defect detection.

The guided wave propagates in the pipe satisfies reciprocity theorem (Fink 1992). The defect serves as a passive source, and it will generate many new conversion modes while reflecting the excitation modes. Employing the time-reversal method for pipe defect detection leads to the guided wave energy focusing on the defect position, and result in the amplitude of the defect detection signal reaching the maximum value (Xu *et al*. 2019).

The transducer array E_N is composed of N transducers that are evenly distributed along the circumferential direction at one end of the pipeline. The ultrasonic guided waves synchronously excited by the transducer array will propagate forward along the pipeline. When ultrasonic guided waves arrive at defect (z_D, θ_D, r_D), scattering and mode conversion will occur. At this moment, the defect can be regarded as a new wave source to emit ultrasonic guided waves outward as reflected wave. The reflected wave will propagate back to the transducer array along the pipeline and be received by the transducers. The signal received by the transducer E_k is as follows

$$S_k(\omega_0) = \sum_{i=1}^{N} H_{Dk}(\omega_0) S_1(\omega_0)\, H_{iD}(\omega_0) \tag{8}$$

where $H_{Dk}(\omega)$ is the transfer function from defect (z_D, θ_D, r_D) to the transducer E_k; $S_1(\omega_0)$ is the Fourier transformation of the initial excitation signal; $H_{iD}(\omega)$ is the transfer function from the transducer E_i to defect (z_D, θ_D, r_D); and N is the number of transducers in the transducer array.

Guided waves propagating in pipelines satisfy reciprocity theorem, based on the time reversal method, we take the complex conjugate of the received signal in the frequency domain where τ is an overall delay necessary to ensure causality, so that the time-reversal signal generated by the received signal at transducer E_k is

$$\begin{aligned} S_{TR,k}(\omega_0) &= e^{i\omega\tau} S_k^*(\omega_0) \\ &= e^{i\omega\tau} \sum_{i=1}^{N} H_{Dk}^*(\omega_0) S_1^*(\omega_0)\, H_{iD}^*(\omega_0) \end{aligned} \tag{9}$$

where "*" denotes the complex conjugate, subscript "*TR*" denotes the time-reversal signal.

A total of N time reversal signals are produced. All of N time-reversal signals are synchronously excited again via corresponding transducers, and the time-reversal focusing signal at defect (z_D, θ_D, r_D) is

$$\begin{aligned} S_D^{TR}(\omega_0) &= \sum_{k=1}^{N} H_{kD}(\omega_0) S_{TR,k}(\omega_0) \\ &= e^{i\omega\tau} \sum_{k=1}^{N} \sum_{i=1}^{N} H_{kD}(\omega_0) H_{Dk}^*(\omega_0) S_1^*(\omega_0)\, H_{iD}^*(\omega_0) \end{aligned} \tag{10}$$

where $H_{kD}(\omega_0)$ is the transfer function from the transducer E_k to defect (z_D, θ_D, r_D).

After time reversal, the final focusing signal received by the entire transducer array can be expressed as

$$\begin{aligned} S_{R,TR}(\omega_0) &= \sum_{i=1}^{N} H_{Di}(\omega_0)\, S_D^{TR}(\omega_0) \\ &= \sum_{i=1}^{N} \sum_{k=1}^{N} H_{Di}(\omega_0)\, S_{TR,k}(\omega_0) H_{kD}(\omega_0) \end{aligned} \tag{11}$$

where $H_{Di}(\omega_0)$ is the transfer function from defect (z_D, θ_D, r_D) to the transducer E_i.

Let

$$S_{ik}^{TR}(\omega_0) = H_{Di}(\omega_0) S_{TR,k}(\omega_0) H_{kD}(\omega_0) \tag{12}$$

The Eq. (11) can be rewritten as

$$S_{R,TR}(\omega_0) = \sum_{i=1}^{N} \sum_{k=1}^{N} S_{ik}^{TR}(\omega_0) \tag{13}$$

It can be seen from Eq. (13), the final focusing signal received by the entire transducer array is the linear superposition of $N \times N$ independent items $S_{ik}^{TR}(\omega_0)$. From Eq. (12), it is clear that each independent item denotes the time reversal signal $S_{TR,k}(\omega_0)$ excited by the transducer E_k, after being reflected by the defect and then received by transducer E_i. That is to say, the final detected signal from multi-channel synchronous excitation system can be decomposed into $N \times N$ independent single-channel signals. Therefore, a simple single-channel apparatus can be

used to replace the complicated multi-channel synchronous excitation system in practice to fulfill the time-reversal method. By repeatedly acquiring the signal from the single-channel apparatus and then taking the linear superposition, the equivalent results of multi-channel synchronous excitation system function is obtained, so as to realize the synthetic time-reversal method.

3. FEM simulation

The schematic of pipe with a single notch defect is shown in Fig. 8. The pipe dimension and material parameters are shown in Table 1.

The notch defect is introduced at 800 mm from one pipe end, and the defect depth is 1 mm with 2 mm axial width and 35 mm circumferential length. Two PZT transducer arrays are axisymmetrically arranged at the end of the pipe to excite and to receive ultrasonic guided wave signals in the process of pipe defect detection.

The ABAQUS software is used for finite element method (FEM) simulation, and the pipe FEM model was built with C3D8R solid unit as shown in Fig. 9(a). Along the pipe circumference 32 elements are divided evenly, and 4 elements are divided along the pipe wall. At the end of pipe FEM model, 32 excitation nodes and 32 receiving nodes at the adjacent 2 mm are placed axisymmetrically. To ensure that there are enough elements in one wavelength and to control the propagation error of guided wave within 0.5%, the element length should satisfy $L < \lambda m/8$, where the λm is the minimum wavelength of excitation signal mode (Deng *et al*. 2010). In this research the element length is selected to be 2 mm, and the FEM simulation time step is 0.1 μs with 120 kHz frequency. With these parameters, the FEM simulation accuracy convergence is satisfactory.

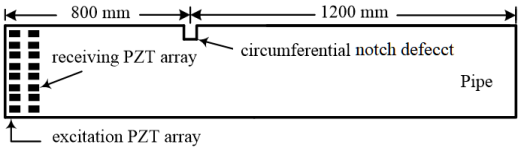

Fig. 8 Schematic of pipe with a single notch defect

As shown in Fig. 9(b), a 120 kHz Hanning windowed 10-cycle sinusoidal signal is applied to all 32 excitation nodes synchronously to excite the L(0,2) mode guided wave in the pipe. When the generated L(0,2) mode guided wave propagates along the pipe with a circumferential notch defect, it will be partially mode converted at the notch defect to give flexural F(n, m) modes such as F(1,3), F(2,3), as well as the longitudinal L(0,1) mode (Tang *et al*. 2007). The individual direct detection signal is shown in Fig. 10.

The deformation of the F(n, m) modes at the axisymmetrical position of pipe is just opposite, so that the F(n, m) conversion modes can be effectively suppressed by summing up all the signals from 32 receiving nodes axisymmetrically placed at the end of the pipe (Jiang *et al*. 2014). The normalized direct detection signal after summing up 32 receiving signals is shown in Fig. 11. We have introduced only one defect in the pipe, there are two detected wave packets in the normalized direct detection signal. According to the group velocity dispersion curves shown in Fig. 2, by analyzing and computing the position of the wave packets, the first wave packet is the L(0,2) reflection mode from the defect, and the second wave packet is the L(0,1) conversion mode produced by the interaction between the incident L(0, 2) mode guided wave and the defect.

It can be seen from Fig. 11 that the two detected wave packets are very small. Such small signals, in practice, are often submerged by noise, and may not be detectable. Using the time-reversal method for pipe defect detection leads to guided wave energy focusing on the defect, result in defect

Table 1 Pipe dimension and material parameters

Pipe dimension			Pipe material		
Length	Outside diameter	Wall thickness	Density	Elastic modulus	Poisson's ratio
2000 *mm*	76 *mm*	4 *mm*	7850 kg/m^3	210 $\times 10^9$ *Pa*	0.28

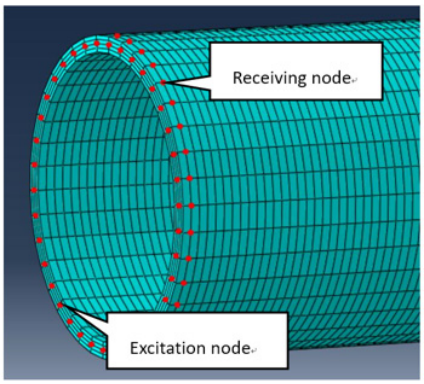

(a) The pipe finite element model

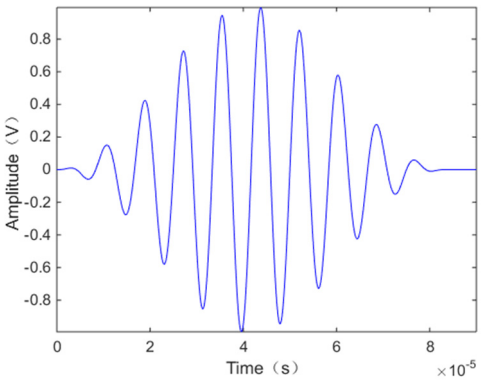

(b) Hanning windowed 10-cycle sinusoidal signal

Fig. 9 The pipe finite element model and excitation signal

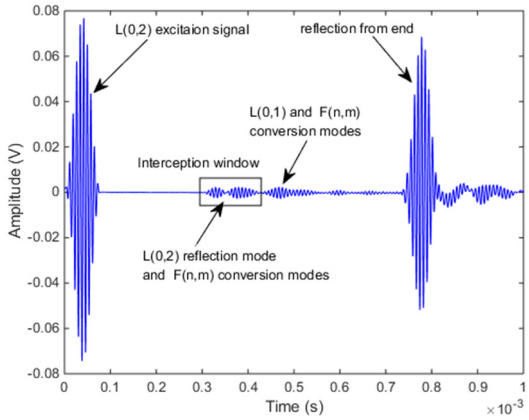

Fig. 10 The typical FEM direct detection signal obtained from individual receiving node

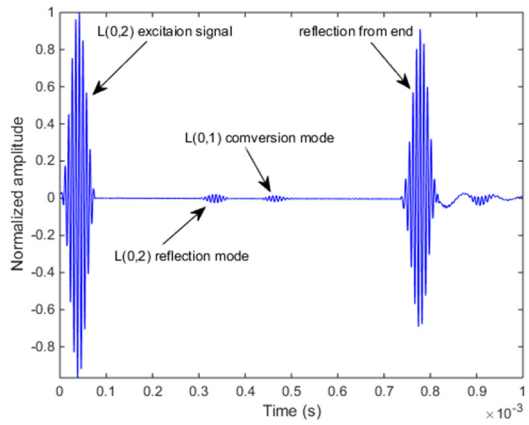

Fig. 11 The FEM normalized direct detection signal

reflection signals being enhanced to a higher level (Deng *et al*. 2010, Zhou 2012). This feature is used to improve the ability of small defects detection. As shown in Fig. 10, an appropriate rectangular window is used for the interception of defect L(0,2) reflection and F(n,m) conversion modes from every individual direct detection signal. The intercepted signal is recorded as $f(t)$. Each $f(t)$ is time reversed to produce the time-reversal signal $f_{TR}(t)$, and these two signals satisfy $f_{TR}(t) = f(\tau\text{-}t)$, where τ is the width of the interception window. A total of 32 time-reversal signals are produced. These time-reversal signals are re-excited from corresponding excitation nodes synchronously, and the reflection signals are obtained from 32 receiving nodes. After summing up all 32 reflection signals, the normalized time-reversal detection signal is obtained, as shown in Fig. 12.

From Fig. 12 we can tell that both L(0,2) and L(0,1) amplitudes of time-reversal detection signals are enlarged as compared with that of direct detection signals, and they are easier to distinguish. Thus, the ability of small defect detection is improved. The comparison of FEM L(0,2) and L(0,1) reflection coefficients between direct detection and time-reversal detection is shown in Table 2.

The reflection coefficient is defined as the ratio of the Peak to Peak value of the reflected signal to that of the excitation signal. Using direct detection method the

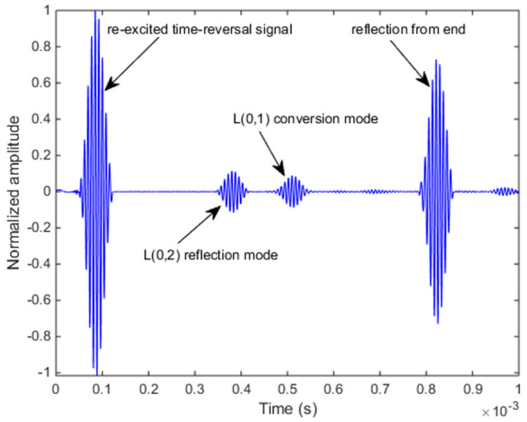

Fig. 12 The FEM normalized time-reversal detection signal

Table 2 Comparison of FEM L(0,2) and L(0,1) reflection coefficients

Reflection coefficient	Direct detection	Time-reversal detection	Times of enhancement
L(0,2)	0.0215	0.1123	5.22
L(0,1)	0.0208	0.1082	5.20

reflection coefficient of L(0,2) or L(0,1) is 0.0215 or 0.0208 respectively. While using time-revers detection method both reflection coefficients are 0.1123 and 0.1082. Times of enhancement for L(0,2) or L(0,1) reflection coefficient is 5.22 or 5.20, both reflection coefficients enhancement are more than 5 times.

4. Experiment

4.1 Pipe with a single defect

An AISI304 steel pipe with the parameters shown in table 1 is used in this research. A single notch defect is introduced at 800 mm from one pipe end, as shown in Fig. 13(a). The defect depth is 1 mm with 2 mm axial width and 35 mm circumferential length. Two PZT transducer arrays are arranged axisymmetrically around the pipe end, and each array is composed of 16 PZT patches as shown in Fig. 13(b).

In this research, several experiments have been employed to strengthen the excitation of L(0,2) mode as well as to restrain that of the L(0,1) mode. We have tested many size of length-expanding and contracting PZT patch. Calculating the L(0,1) mode wave length according to equation (7), the PZT patch size is finally chosen as $16mm \times 3mm \times 1mm$, and the distance between the two transducer arrays is 1mm (Alleyne and Cawley 1996, 1997). It is validated that with this size of PZT patch, the single pure L(0,2) mode guided waves can be generated in the pipe, and the flexural F(n,m) modes are also minimized by applying a Hanning windowed toneburst signal centered on the 120 kHz frequency to the transducer array. The properties of piezoelectric material for PZT patch are shown in Table 3.

(a) A single notch defect in pipe (b) The transducer array layout

Fig. 13 Pipe with a single notch defect and the transducer array layout

Table 3 Properties of piezoelectric material for PZT patch

Parameter	Symbol	Value	Unit
Piezoelectric constants	e_{31}	*-5.2*	*C/m2*
Piezoelectric charge constants	d_{31}	*-123*	*pm/v*
Density	ρ	*7500*	kg/m^3
Frequency constant	*N*	*2*	*MHz • mm*
Length of piezoelectric material	*L*	*16*	*mm*
Width of piezoelectric material	*W*	*3*	*mm*
Thickness of piezoelectric material	*T*	*1*	*mm*

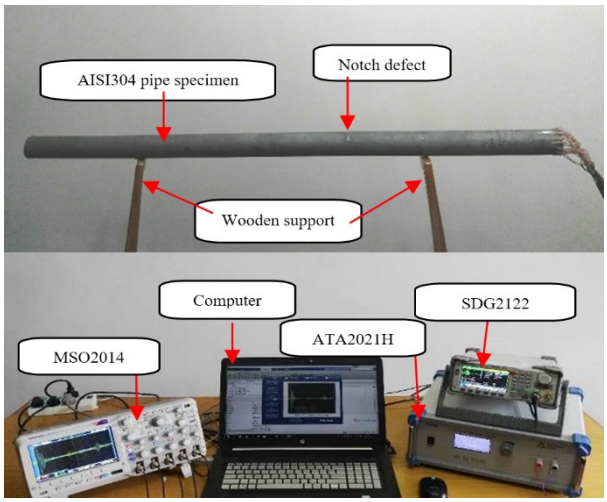

Fig. 14 Experimental setup

The experimental setup is shown in Fig. 14. The AISI304 pipe specimen is rested on a wooden support. The Siglent SDG2122 arbitrary waveform generator is employed to generate a 120 kHz Hanning windowed 10-period sinusoidal signal. This signal is amplified to 100 Vpp by the Agitek ATA2021H power amplifier, and then is applied to the excitation transducer array to generate L(0,2) mode guided wave in the pipe. The reflection signal is detected by the receiving transducer array, the Tektronix MSO2014 digital oscilloscope is used to collect the reflection signal, and the computer is utilized for data processing. The following are the experiment steps.

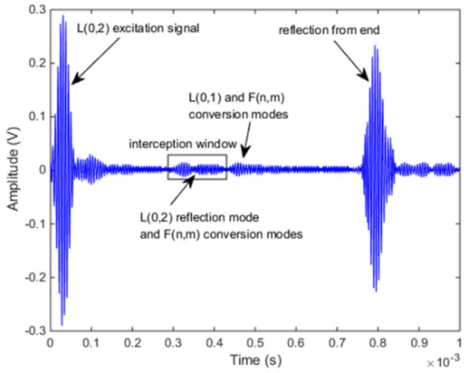

Fig. 15 The experimental direct detection signal obtained from individual receiving PZT transducer

Step 1: An 120 kHz Hanning windowed 10-period sinusoidal signal is applied to the excitation PZT array, and 16 defect reflection signals from the receiving PZT array are recorded by the digital oscilloscope. The individual direct detection signal is shown in Fig. 15.

After summing up all 16 individual receiving signals, the F(n,m) conversion modes are suppressed, and the experimental normalized direct detection signal is shown in Fig. 16. Although we have only introduced one defect in the pipe, there are two detected wave packets in the experimental normalized direct detection signal. By analyzing and computing the position of the wave packets with the same approach as FEM simulation, the first wave packet is the L(0,2) reflection mode from the defect, the second wave packet is the L(0,1) conversion mode produced by the interaction between the incident L(0, 2) mode guided wave and the defect in the pipe. Both L(0,2) and L(0,1) wave packets are quite small and may not be distinguished with noise in practice. To improve the ability of small defect detection, the synthetic time-reversal method is utilized in the next experiment steps.

Step 2: As shown in Fig. 15, an appropriate rectangular window is used to intercept the defect L(0,2) reflection and F(n,m) conversion modes from every individual direct detection signal. The intercepted signal is time reversed to produce the time-reversal signal, a total of 16 time-reversal signals are produced. Each time-reversal signal is re-excited from corresponding excitation PZT transducer with the

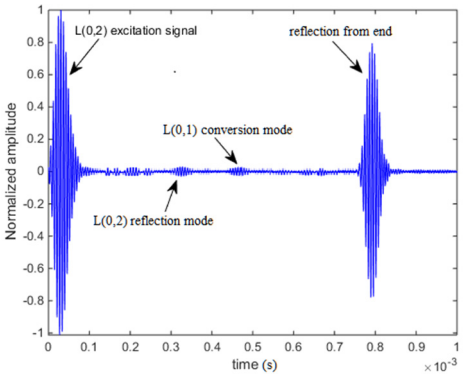

Fig. 16 The experimental normalized direct detection signal

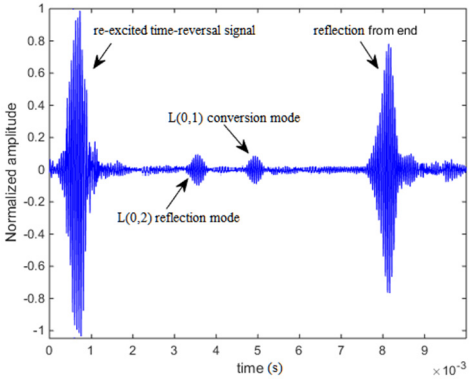

Fig. 17 The experimental normalized time-reversal detection signal

same circumferential position of the receiving transducer, totally re-excite 16 times. After each excitation, 16 reflection signals are recorded from the receiving PZT array by the digital oscilloscope.

Step 3: The 16×16 reflection signals from the receiving PZT array are summed up to obtain the equivalent multi-channel synchronous excitation time-reversal detection signal. The experimental normalized time-reversal detection signal is shown in Fig. 17. It is clear that both L(0,2) and L(0,1) amplitudes of time-reversal detection signals are enhanced to a higher level, and they are easier to identify in practice.

The comparison of experimental L(0,2) and L(0,1) reflection coefficients between the direct detection and the time-reversal detection is shown in Table 4. The enhancement of both reflection coefficients is about 5 times. The experimental result is in good agreement with FEM simulation.

Table 4 Comparison of experimental L(0,2) and L(0,1) reflection coefficients

Reflection coefficient	Direct detection	Time-reversal detection	Times of enhancement
L(0,2)	0.0211	0.1057	5.01
L(0,1)	0.0208	0.1040	5.00

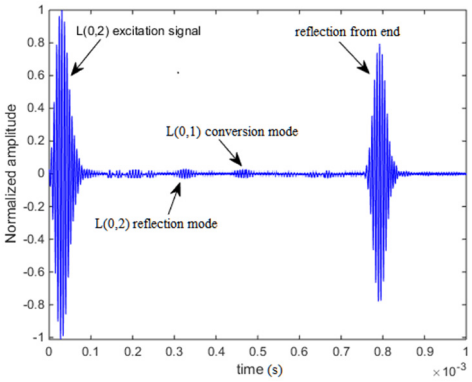

(a) 1 mm defect depth

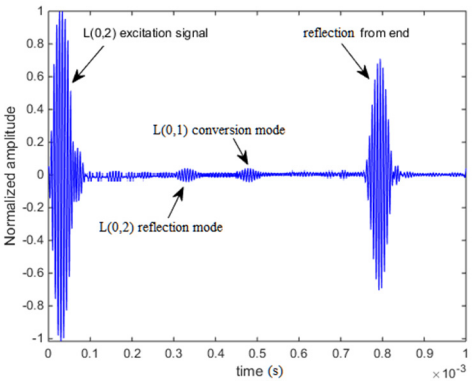

(b) 2 mm defect depth

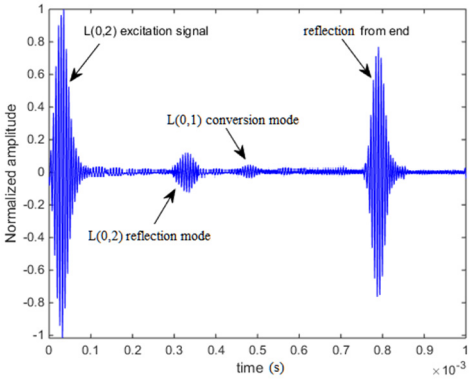

(c) 3 mm defect depth

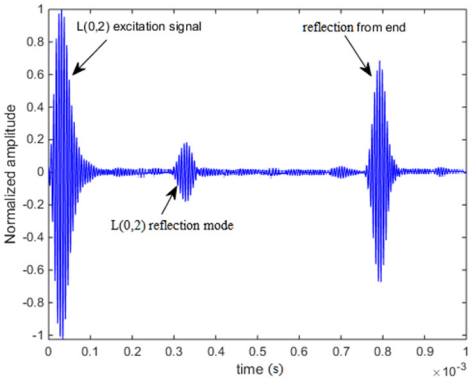

(d) 4 mm defect depth

Fig. 18 The experimental normalized direct detection signals with different defect depth

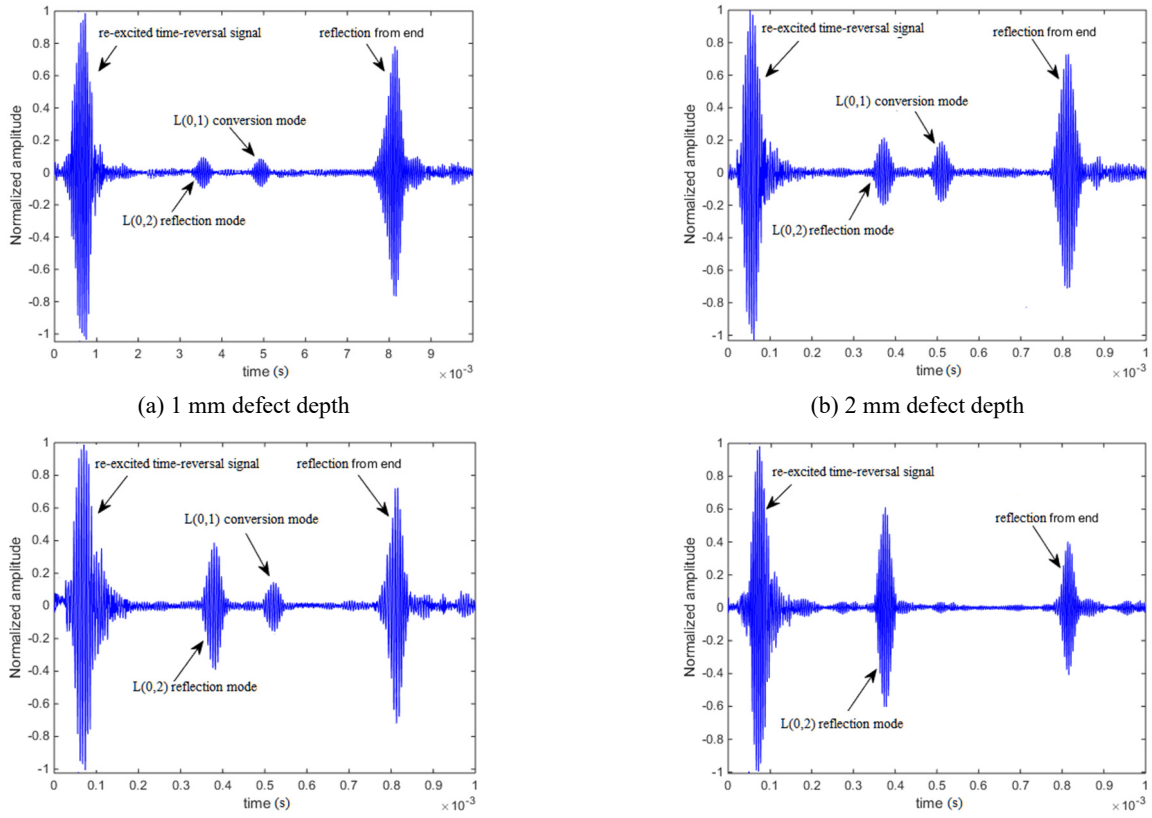

(a) 1 mm defect depth

(b) 2 mm defect depth

(c) 3 mm defect depth

(d) 4 mm defect depth

Fig. 19 The experimental normalized time-reversal detection signals with different defect depth

Table 5 Comparison of experimental L(0,2) and L(0,1) reflection coefficients with different defect depth

Defect depth	Signal mode	Reflection coefficients		Times of enhancement
		Direct detection	Time-reversal detection	
1 mm	L(0,2)	0.0201	0.1031	5.11
	L(0,1)	0.0197	0.0995	5.05
2 mm	L(0,2)	0.0452	0.2158	4.79
	L(0,1)	0.0431	0.2102	4.87
3 mm	L(0,2)	0.0843	0.3881	4.61
	L(0,1)	0.0398	0.1891	4.75
4 mm	L(0,2)	0.1304	0.5998	4.60
	L(0,1)	0	0	0

4.2 Pipe with defect of different depth

A single notch defect is introduced at 800 mm from the AISI304 steel pipe end. The defect axial width is 2 mm with 35 mm circumferential length, and the defect depth expands from 1 mm to 4 mm. The direct detection signals and the time-reversal detection signals are shown in Figs. 18 and 19, respectively. With the defect depth increase, the amplitude of L(0,1) increase first, then decrease, and at last reaches zero, while the amplitude of L(0,2) increase monotonously. The experimental result is consistent with the analyzing of the influence of defect depth on L(0,2) to L(0,1) mode conversion in section 2.2. The amplitudes variation trend of L(0,2) and L(0,1) with different defect depth provides an important reference for pipeline defect depth identification.

The comparison of experimental L(0,2) and L(0,1) reflection coefficients between direct detection and time-reversal detection with different defect depth is shown in Table 5. It is obvious that the reflection coefficients of time-reversal detection signals are larger than that of direct detection signals, especially for the small defect in the early crack stage. The smaller the defect is, the more enhancement of the reflection coefficients occurs. This feature makes it easier to distinguish the small pipeline defects.

5. Discussion

Minor defects in pipeline only introduce weak reflections of guided wave, which limits the detection range and make it ineffective to use guided wave signals for reliable pipeline defect detection. To enhance the inspection potential ability of guided waves for small defect, time-reversal method has been introduced to the field of pipeline defect detection and found effective in a solid circular waveguide for the dispersed multi-mode signals. When the excited L(0,2) mode guided wave propagates along a pipeline with defect, the echo signals will contain the L(0,2) reflection mode and other conversion modes including the L(0,1) mode. Using the time-reversal method for pipeline

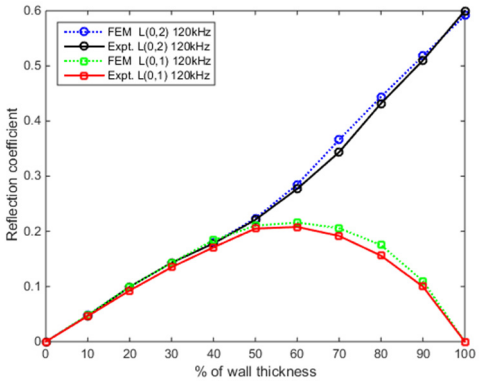

Fig. 20 Variation trend of L(0,2) and L(0,1) reflection coefficients with different defect depth, (defect circumferential length is fixed to 20% circumference)

defect detection, the amplitudes of L(0,2) and L(0,1) mode reflection signals at the defect are enhanced to a higher level, so as to distinguish the small defect more easily. In addition to the L(0,2) reflection mode, the L(0,1) conversion mode also contain useful information in the process of pipeline defect detection.

5.1 The L(0,2) and L(0,1) reflection characteristics with different defect depth

To evaluate quantitatively the pipeline defect depth identification with L(0,2) and L(0,1) reflection coefficients, the defect circumferential length is fixed to 20% of circumference, and the defect depth is divided into 10 grades, from 10% to 100% of wall thickness with an increment of 10%. With the 120 kHz excitation signal, the FEM simulation and the experiment of time-reversal defect detection are carried out, and the results of L(0,2) and L(0,1) reflection coefficients with different defect depth are shown in Fig. 20.

The circular annotated curves are L(0,2) reflection coefficients, the square annotated curves are L(0,1) reflection coefficients. Meanwhile, the solid lines denote the experimental results, and the dotted lines denote the numerical simulation results. It is clear that the FEM simulation are in good agreement with the experimental results.

With increase of defect depth, the L(0,2) reflection coefficient increases monotonously, while the L(0,1) reflection coefficient increases first, and then decreases. Before the defect reaches half-wall-thickness, the L(0,2) and the L(0,1) reflection coefficients are almost the same. When the defect depth reaches half-wall-thickness, the L(0,1) reflection coefficient reaches the maximum value. As the defect depth extends further, the L(0,1) reflection coefficient gradually decreases while the L(0,2) reflection coefficient still increases. When the defect depth reaches through-thickness, the L(0,1) reflection coefficient decreases to zero, and the L(0,2) reflection coefficient reaches the maximum value. This feature is significant for pipeline defect depth identification.

By fitting the experimental data of L(0,2) or L(0,1) reflection coefficient with defect depth using the least squares method, the following theoretical equations are obtained, which can be used to evaluate quantitatively the defect depth of the tested pipe.

$$\begin{cases} R_{L2} = 0.0057x - 0.029 \\ R_{L1} = 0.00003x^2 - 0.0043x - 0.0014 \end{cases} \tag{14}$$

Where R_{L2} or R_{L1} is the L(0,2) or L(0,1) reflection coefficient respectively, and x is the percentage of defect depth along wall thickness.

5.2 The L(0,2) and L(0,1) reflection characteristics with different defect circumferential length

The defect depth is fixed to 70% of wall thickness, and the defect circumferential length is divided into 10 grades, from 10% to 100% of the circumference with an increment of 10%. With the 120 kHz excitation signal, the FEM simulation and the experiment of time-reversal defect detection are carried out, and the results of L(0,2) and L(0,1) reflection coefficients with different defect circumferential length are shown in Fig. 21.

The L(0,2) and L(0,1) reflection coefficients are nonlinearly increasing with the defect circumferential length. At the beginning, the rate of increase is larger, then gradually saturating. This is because the time-reversal method is used to conduct guided wave detection, and the energy of the guided wave will focus on the defect. The guided wave energy gradually disperse with the increase of the defect circumferential length, and result in its distribution in the circumferential direction inconsistent. With the defect circumferential length extends further, the energy of the guided wave will be distributed uniformly throughout the circumference of the pipe when the defect circumferential length reaches full circumference.

The defect depth is fixed to 100% of wall thickness, with the 120 kHz excitation signal, the L(0,2) and L(0,1) reflection coefficients with different defect circumferential length are shown in Fig. 22.

The L(0,2) reflection coefficients increases nonlinearly with the defect circumferential length, while the L(0,1)

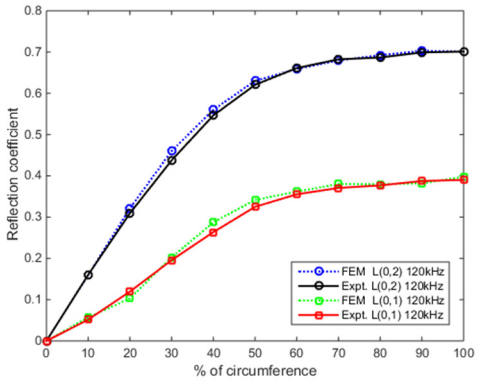

Fig. 21 Variation trend of L(0,2) and L(0,1) reflection coefficients with different defect circumferential length, (defect depth is fixed to 70% of wall thickness)

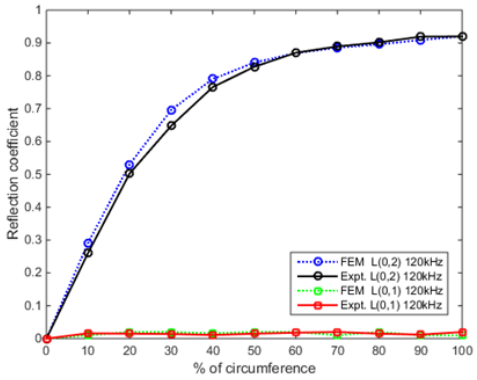

Fig. 22 Variation trend of L(0,2) and L(0,1) reflection coefficients with different defect circumferential length, (defect depth is fixed to 100% of wall thickness)

reflection coefficient is approximately zero. This feature indicates that the L(0,2) mode will not be converted to L(0,1) mode at a through-thickness defect, and it is another important reference for pipeline defect depth identification.

6. Conclusions

In this paper, the time-reversal technology in pipeline defect detection is investigated by FEM simulation and experiments, and a new approach of pipe defect depth identification is proposed. The following are some important conclusions drawn from this research.

- The ability of pipeline defect detection is effectively improved by using the time-reversal method, especially for the small defect in the early crack stage. Utilizing the PZT transducer array and the principle of linear superposition, the equivalent function of multi-channel synchronous excitation time-reversal detection is realized by using a single-channel apparatus with synthetic time-reversal method.
- When the excited L(0,2) mode guided wave propagates along the pipeline with a circumferential notch defect, the L(0,2) mode will be partially converted to other modes including the L(0,1) mode. If the defect is through-thickness, the L(0,1) mode will not be converted.
- In addition to the L(0,2) reflection mode, the L(0,1) conversion mode also contain useful pipeline defect information. With almost the same L(0,2) and L(0,1) reflection coefficients, the defect depth have not reached half-wall-thickness. When the L(0,1) reflection coefficient reaches the maximum value, the defect depth reaches half-wall-thickness. When the L(0,1) reflection coefficient begin to decrease, the defect depth reaches over half-wall-thickness. When the L(0,1) reflection coefficient reaches zero while that of L(0,2) reaches the maximum value, the defect depth reaches through-thickness. The defect depth can be easily identified by monitoring the variation trend of L(0,2) and L(0,1) reflection coefficients, and using Eq. (14) the defect depth of the tested pipe could be evaluated quantitatively.

Acknowledgments

The research described in this paper was financially supported by the National Natural Science Foundation of China (grant number 52078052), and the China National Petroleum Corporation Essential Research and Strategic Reserve Technology Research Fund Project (grant number 2017Z-05).

References

Alleyne, D.N. and Cawley, P. (1996), "The excitation of Lamb waves in pipes using dry-coupled piezoelectric transducers", *J. Nondestr. Eval.*, **15**(1), 11-20. https://doi.org/10.1007/BF00733822

Alleyne, D.N. and Cawley, P. (1997), "Long range propagation of Lamb waves in chemical plant pipe work", *Mater. Eval.*, **7**, 504-508. https://doi.org/10.1016/S1044-5803(97)00084-3

Beena, K., Shruti, S., Sandeep, S. and Naveen, K. (2017), "Monitoring degradation in concrete filled steel tubular sections using guided waves", *Smart Struct. Syst., Int. J.*, **19**(4), 371-382. https://doi.org/10.12989/sss.2016.19.4.371

Cahill, P., Pakrashi, V. and Sun, P. (2018), "Energy harvesting techniques for health monitoring and indicators for control of a damaged pipe structure", *Smart Struct. Syst., Int. J.*, **21**(3), 287-303. https://doi.org/10.12989/sss.2018.21.3.287

Cassereau, D. and Fink, M. (1992), "Time-reversal of ultrasonic fields. III. Theory of the closed time-reversal cavity", *IEEE Transact. Ultrason. Ferroelectr. Freq. Control*, **39**(5), 579-592. https://doi.org/10.1109/58.156176

Cawley, P., Lowe, M.S., Simonetti, F., Chevalier, C. and Roosenbrand, A.G. (2002), "The variation of the reflection coefficient of extensional guided waves in pipes from defects as a function of defect depth, axial extent, circumferential extent and frequency", *Proceedings of the Institution of Mechanical Engineers Part C, Journal of Mechanical Engineering Science*, **216**(11), 1131-1143. https://doi.org/10.1243/095440602761609498

Deng, F., Wu, B. and He, C.F. (2010), "Time reversal guided wave defect identification method", *J. Mech. Eng.*, **46**(8), 18-24. https://doi.org/10.3901/JME.2010.08.018

Ditri, J.J. (1994), "Utilization of guided elastic waves for the characterization of circumferential cracks in hollow cylinders", *J. Acoust. Soc. Am.*, **96**(6), 3769-3775. https://doi.org/10.1121/1.410565

Du, G., Kong, Q., Wu, F., Ruan, J. and Song, G. (2016), "An experimental feasibility study of pipeline corrosion pit detection using a piezoceramic time reversal mirror", *Smart Mater. Struct.*, **25**(3), 037002. https://doi.org/10.1088/0964-1726/25/3/037002

Du, G., Kong, Q., Zhou, H. and Gu, H. (2017), "Multiple cracks detection in pipeline using damage index matrix based on piezoceramic transducer-enabled stress wave propagation", *Sensors*, **17**(8), 1812. https://doi.org/10.3390/s17081812

Feng, Q., Kong, Q., Tan, J. and Song, G. (2017), "Grouting compactness monitoring of concrete-filled steel tube arch bridge model using piezoceramic-based transducers", *Smart Struct. Syst., Int. J.*, **20**(2), 175-180. https://doi.org/10.12989/sss.2017.20.2.175

Fink, M. (1992), "Time reversal of ultrasonic fields. I. Basic

principles", *IEEE Transact. Ultrason. Ferroelectr. Freq. Control*, **39**(5), 555-566. https://doi.org/10.1109/58.156174

Fitch, A.H. (1963), "Observation of elastic-pulse propagation in axially symmetric and non-axially symmetric longitudinal modes of hollow cylinders", *J. Acoust. Soc. Am.*, **35**(5), 706-708. https://doi.org/10.1121/1.1918594

Fu, H., Wu, B. and He, C.F. (2013), "Ultrasonic Guided wave pipe inspection based on synthetic time-reverse method", *J. Mech. Eng.*, **49**(12), 17-23. https://doi.org/10.3901/JME.2013.12.017

Gao, Q., Wang, B.Z. and Wang, X.H. (2015), "Far-field super-resolution imaging with compact and multifrequency planar resonant lens based on time reversal", *IEEE Transact. Antennas Propag.*, **63**(12), 5586-5592. https://doi.org/10.1109/TAP.2015.2496098

Garg, M., Sharma, S., Sharma, S. and Mehta, R. (2016), "Non-contact damage monitoring technique for FRP laminates using guided waves", *Smart Struct. Syst.*, *Int. J.*, **17**(5), 795-817. https://doi.org/10.12989/sss.2016.17.5.795

Gazis, D.C. (1958), "Exact analysis of the plane-strain vibrations of thick-walled hollow cylinders", *J. Acoust. Soc. Am.*, **30**, 786-794. https://doi.org/10.1212/1.1909761

Gazis, D.C. (1959a), "Three-dimensional investigation of the propagation of waves in hollow circular cylinders. I. analytical foundation", *J. Acoust. Soc. Am.*, **31**(5), 568-573. https://doi.org/10.1121/1.1907753

Gazis, D.C. (1959b), "Three-dimensional investigation of the propagation of waves in hollow circular cylinders. II. numerical results", *J. Acoust. Soc. Am.*, **31**(5), 573-578. https://doi.org/10.1121/1.1907754

Giannelli, P., Bulletti, A. and Capineri, L. (2017), "Multifunctional piezopolymer film transducer for structural health monitoring applications", *IEEE Sensors J.*, **17**(14), 4583-4586. https://doi.org/10.1109/JSEN.2017.2710425

Gomez, C.Q., Garcia, F.P., Arcos, A., Cheng, L., Kogia, M. and Papelias, M. (2017), "Calculus of the defect severity with EMATs by analysing the attenuation curves of the guided waves", *Smart Struct. Syst.*, *Int. J.*, **19**(2), 195-202. https://doi.org/10.12989/sss.2017.19.2.195

Hong, X., Song, G., Ruan, J., Zhang, Z., Wu, S. and Liu, G. (2016a), "Active monitoring of pipeline tapered thread connection based on time reversal using piezoceramic transducers", *Smart Struct. Syst.*, *Int. J.*, **18**(4), 643-662. https://doi.org/10.12989/sss.2016.18.4.643

Hong, X., Ruan, J., Liu, G., Wang, T., Li, Y. and Song, G. (2016b), "Synergetics based damage detection of frame structures using piezoceramic patches", *Smart Struct. Syst.*, *Int. J.*, **17**(2), 167-194. https://doi.org/10.12989/sss.2016.17.2.167

Hosseinabadi, H.Z., Nazari, B., Amirfattahi, R., Mirdamadi, H.R. and Sadri, A.R. (2014), "Wavelet network approach for structural damage identification using guided ultrasonic waves", *IEEE Transact. Instrument. Measure.*, **63**(7), 1680-1692. https://doi.org/10.1109/TIM.2014.2299528

Huo, L., Wang, F., Li, H. and Song, G. (2017), "A fractal contact theory based model for bolted connection looseness monitoring using piezoceramic transducers", *Smart Mater. Struct.*, **26**(10), 104010. https://doi.org/10.1188/1361-665X/aa6e93

Ing, R.K. and Fink, M. (1998), "Time-reversed Lamb waves", *IEEE Transact. Ultrason. Ferroelectr. Freq. Control*, **45**(4), 1032-1043. https://doi.org/10.1109/58.7105866

Jiang, Y., Jing, R.,Yan, Y., Guo, Z., Chen, L. and Gao, S. (2014), "Experimental study of signal identification on crack and corrosion with ultrasonic guided wave", *Chinese Mech. Sci. Technol. Aerosp. Eng.*, **33**, 551-554. https://doi.org/10.13433/j.cnki.1003-8728.2014.04.020

Jiang, T., Kong, Q., Patil, D., Luo, Z., Huo, L. and Song, G. (2017), "Detection of debonding between fiber reinforced polymer bar and concrete structure using piezoceramic transducers and wavelet packet analysis", *IEEE Sensors J.*, **17**(7), 1992-1998. https://doi.org/10.1109/JSEN.2017.2660301

Leutenegger, T. and Dual, J. (2002), "Detection of defects in cylindrical structures using a time reverse method and a finite-difference approach", *Ultrasonics*, **40**(1), 721-725. https://doi.org/10.1016/S0041-624X(02)00200-7

Li, J., Hao, H., Xia, Y. and Zhu, H.P. (2014), "Damage detection of shear connectors in bridge structures with transmissibility in frequency domain", *Int. J. Struct. Stabil. Dyn.*, **14**(02), 1350061. https://doi.org/10.1142/S0219455413500612

Li, L., Mei, H., Haider, M.F., Rizos, D., Xia, Y. and Giurgiutiu, V. (2020), "Guided wave field calculation in anisotropic layered structures using normal mode expansion method", *Smart Struct. Syst.*, *Int. J.*, **26**(2), 157-174. https://doi.org/10.12989/sss.2020.26.2.157

Liao, T.H., Hsieh, P.C. and Chen, F.C. (2009), "Subwavelength target detection using ultrawideband time-reversal techniques with a multilayered dielectric slab", *IEEE Antennas Wireless Propag. Lett.*, **8**, 835-838. https://doi.org/10.1109/LAWP.2009.2025897

Lu, G., Li, Q. Y., Wang, H. and Song, G. (2017), "Characterization of ultrasound energy diffusion due to small-size damage on an aluminum plate using piezoceramic transducers", *Sensors*, **17**(12), 2796. https://doi.org/10.3390/s17122796

Luo, M., Li,W., Hei, C. and Song, G. (2016), "Concrete infill monitoring in concrete-filled FRP tubes using a PZT-based ultrasonic time-of-flight method", *Sensors*, **16**(12), 2083. https://doi.org/10.3390/s16122083

Lovstad, A. and Cawley, P. (2011), "The reflection of the fundamental torsional guided wave from multiple circular holes in pipes", *NDT & E Int.*, **44**(7), 553-562. https://doi.org/10.1016/j.ndteint.2011.05.010

Lowe, M.S., Alleyne, D.N. and Cawley, P. (1998a), "Defect detection in pipes using guided waves", *Ultrasonics*, **36**(1-5):147-154. https://doi.org/10.1016/S0041-624X(97)00038-3

Lowe, M.S., Alleyne, D.N. and Cawley, P. (1998b), "The mode conversion of a guided wave by a part-circumferential notch in a pipe", *J. Appl. Mech.*, **65**(3), 649-656. https://doi.org/10.1115/1.2789107

May, F. and Dual, J. (2006), "Focusing of pulses in axially symmetric elastic tubes with fluid filling and piezo actuator by a finite difference simulation and a method of time reversal", *Wave Motion*, **43**(4), 311-322. https://doi.org/10.106/j.wavemoti.2006.01.004

Niu, X., Marques, H.R. and Chen, H.P. (2018), "Sensitivity analysis of circumferential transducer array with T(0,1) mode of pipes", *Smart Struct. Syst.*, *Int. J.*, **21**(6), 761-776. https://doi.org/10.12989/sss.2018.21.6.761

Núñez, I. and Negreira, C. (2005), "Efficiency parameters in time reversal acoustics: Applications to dispersive media and multimode wave propagation", *J. Acoust. Soc. Am.*, **117**(3), 1202-1209. https://doi.org/10.1121/1.1856272

Ratassepp, M., Fletcher, S. and Lowe, M.S. (2010), "Scattering of the fundamental torsional mode at an axial crack in a pipe", *J. Acoust. Soc. Am.*, **127**(2), 730-740. https://doi.org/10.1121/1.3277185

Tang, L.G., Cheng, J.C. and Xu, X.M. (2007), "Mechanism of the excitation of single pure mode L(0,2) and its interaction with the defect in a hollow cylinder", *Chinese Phys.*, **16**(4), 1062-1071. https://doi.org/10.1088/1009-1963/16/4/034

Wang, Y. and Hao, H. (2014), "Modelling of guided wave propagation with spectral element: application in structural engineering", *Appl. Mech. Mater.*, **553**, 687-692. https://doi.org/10.4028/www.scientific.net/AMM.553.687

Wang, Y., Zhu, X., Hao, H. and Ou, J. (2009), "Guided wave propagation and spectral element method for debonding damage assessment in RC structures", *J. Sound Vib.*, **324**(3), 751-772.

https://doi.org/10.1016/j.jsv.2009.02.028
Wang, X., Tse, P.W., Mechefske, C.K. and Hua, M. (2010), "Experimental investigation of reflection in guided wave-based inspection for the characterization of pipeline defects", *NDT & E Int*., **43**(4), 365-374. https://doi.org/10.1016/j.ndteint.2010.01.002
Wang, F., Ho, M. and Song, G. (2019), "Monitoring of Early Looseness of Multi-Bolt Connection: A New Entropy-based Active Sensing Method Without Saturation", *Smart Mater. Struct*., **28**(10), 10LT01. https://doi.org/10.1188/1361-665X/ap3a08
Wu, F., Thomas, J.L. and Fink, M. (1992), "Time reversal of ultrasonic fields. II. Experimental results", *IEEE Transact. Ultrason. Ferroelectr. Freq. Control*, **39**(5), 567-578. https://doi.org/10.1109/58.156175
Xu, Y., Luo, M., Hei, C. and Song, G. (2018), "Quantitative evaluation of compactness of concrete-filled fiber-reinforced polymer tubes using piezoceramic transducers and time difference of arrival", *Smart Mater. Struct*., **27**, 035023. https://doi.org/10.1088/1361-665X/aa9dd0
Xu, Y., Luo, M., Liu, Q., Du, G. and Song, G. (2019), "PZT transducer array enabled pipeline defect locating based on time-reversal method and matching pursuit de-noising", *Smart Mater. Struct*., **28**, 075019. https://doi.org/10.1088/1361-665X/ab1cc9
Yan, S., He, B.B. and Zhao, N.Z. (2012), "Experimental validation and plotting guided wave dispersion curve of pipe structure", *Chin. Eng. Mech*., **29**, 159-163. https://doi.org/10.6052/j.issn.1000-4750.2011.11.S046
Yan, S., Zhang, B., Song, G. and Lin, J. (2018), "PZT-based ultrasonic guided wave frequency dispersion characteristics of tubular structures for different interfacial boundaries", *Senssxp dors*, **18**(12), 4111. https://doi.org/10.3390/s18124111
Zadeh, J.E., Dehmollaian, M. and Aghdam, K.M. (2016), "Electromagnetic time-reversal imaging of pinholes in pipes", *IEEE Transact. Antennas Propag*., **64**(4), 1356-1363. https://doi.org/10.1109/TAP.2016.2526043
Zhang, W., Hao, H., Wu, J., Li, J., Ma, H. and Li, C. (2018), "Detection of minor damage in structures with guided wave signals and nonlinear oscillator", *Measurement*, **122**, 532-544. https://doi.org/10.1016/j.measurement.2017.06.033
Zhou, J.J. (2012), "Development and application of guided wave inspection device based on time reversal method", Ph.D. Dissertation; College of Mechanical Engineering & Applied Electronics Technology, Beijing University of Technology, Beijing, China.